Solid State Ionics 16 (1985) 211-224
North-Holland Publishing Company

ELECTRICAL CONDUCTIVITY AND DEFECT CHEMISTRY OF THE SYSTEM $(Tb_xGd_{1-x})_2Zr_2O_{7+y}$ $(0 \leq x \leq 1; 0 \leq y < 0.25)$

M.P. VAN DIJK, K.J. DE VRIES and A.J. BURGGRAAF

Twente University of Technology, Department of Chemical Engineering, Laboratory for Inorganic Materials Science, P.O. Box 217, 7500 AE Enschede, The Netherlands.

Structural and electrical properties of the homogeneous solid solution series $(Tb_xGd_{1-x})_2Zr_2O_{7+y}$ $(0 \leq x \leq 1; 0 \leq y < 0.25)$ were investigated. The defect structure and electrical properties were studied by thermogravimetric analysis and electrical conductivity and ionic transport number measurements as a function of temperature and oxygen partial pressure. The (p-type) electronic conductivity was found to arise from a small polaron hopping mechanism on the Tb-sublattice. The charge carrier concentration can be correlated with the Tb^{4+} concentration. The maximum fraction of Tb^{4+} ions on the Tb-sublattice was found to be 0.25 and is hardly dependent on the composition (x). Charge carrier mobilities are in the range 10^{-10} - 10^{-8} m^2/Vs at 700°C. Ionic conductivities up to 7×10^{-1} Ω^{-1} m^{-1} at 700°C are found. The conductivity can well be described with a previous developed model, that relates the effects of pyrochlore order in the fluorite lattice with the conductivity parameters.

1. INTRODUCTION

1.1. Use of mixed conducting oxides.

Oxygen ion conducting solid electrolytes are frequently used in applications such as oxygen-sensors, -pumps and fuel cells and may find application in electrocatalytic reactors. In most of these applications noble metals like platinum are used as electrode, especially in the temperature range between 600 and 1000°C. At the electrode the solid-gas interfacial reaction takes place, preferably with low polarization losses and, in case of sensors, fast response times. Platinum is thought to promote the adsorption of gaseous oxygen and to catalyse the interfacial charge transfer reaction:

$$O_{ads} + V_O^{\cdot\cdot} + 2e' \rightleftharpoons O_O^X \qquad (1)$$

The last process is generally believed to take place at the three phase line between the solid electrolyte, the porous electrodematerial and the gas phase. Consequently, this implies that the effective surface area for charge transfer is rather small, compared to the total electrolyte surface, resulting in limited values of the current density. Moreover, the kinetics of the electrode reaction (1) on Pt-electrodes at temperatures below about 600°C is rather slow and becomes rate determining. Finally, noble metal electrodes become unstable at higher temperatures. Hence, it is worthwhile to investigate other possible electrode materials.

In the literature it has been suggested that electronic contributions to the conductivity of the solid electrolyte may improve the performance of noble metal electrodes or can even substitute these[1-4]. It is supposed that a mixed conducting surface layer enhances the number of sites for adsorption of gaseous oxygen and facilitates the charge transfer process, which results in lower polarization losses. In the case of electrocatalytically active materials the activity or selectivity for adsorption and surface reactions might be increased under polarized conditions of the electrode.

0 167-2738/85/$ 03.30

If the mixed conducting surface layer is used in addition to the noble metal electrode, this noble metal still serves as the current collector. In the case where the mixed conductor, in either a porous or dense form, substitutes the noble metal electrode, these current collecting properties should be overtaken. In this case the electronic part of the total conductivity should preferably be much higher than the ionic part in order to establish a constant surface potential across the total electrode area.

In our laboratory properties of mixed conducting materials are investigated and the use of these materials as surface layers on solid electrolytes is explored. The bulk electrical properties of the materials are related to the electrode performance. This paper deals with the bulk properties of one such a system.

1.2. Material system.

Promising materials for use as mixed conducting surface layers on solid electrolytes will be compounds that are compatible with the solid electrolyte, i.e. compounds that have similar composition and structure, resulting in good adherency and equal thermal stability. In this paper we present results of investigations on the system $(Tb_xGd_{1-x})_2Zr_2O_{7+y}$, having in mind $Gd_2Zr_2O_7$ as the solid electrolyte. Compounds of this kind are abbreviated as TGZ(100.x), so TGZ0 stands for $Gd_2Zr_2O_7$).

The oxygen ion conductivity of $Gd_2Zr_2O_7$ is in the same order of magnitude as of the well known yttria stabilized zirconia solid solutions in the temperature range below 700°C[5,6]. This is especially due to the low activation enthalpy (80-85 kJ/mol) for $Gd_2Zr_2O_7$, that can be related to ordering phenomena in the fluorite structure[7,8]. Below the order-disorder transition temperature (≈1550°C[9]) the pyrochlore structure is found with stoichiometry $A_2B_2O_7$. This is effectively a domain-like, ordered superstructure of the defect fluorite structure. Specimen that are quenched from above the order-disorder temperature show the disordered fluorite structure in X-ray diffraction analysis. Nevertheless, indications of local ordering phenomena are apparent from electron diffraction experiments[7]. These specimen have a much higher activation enthalpy for ionic conductivity (≈115 kJ/mol).

Terbium is the neighbour of Gd in the lanthanide series and it can be substituted for Gd quite well. So a series of homogeneous solid solutions between the end members $Gd_2Zr_2O_7$ and $Tb_2Zr_2O_{7+y}$ may be expected. By X-ray diffraction analysis, $Tb_2Zr_2O_{7+y}$ does not show the pyrochlore structure, but similar short-range order phenomena have been observed as are found in quenched $Gd_2Zr_2O_7$[6,7].

Terbium, unlike gadolinium, can be present simultaneously in 3+ as well as in 4+ valence states, thus generating the possibility for electronic conductivity. The stoichiometry of the compounds (the value of y) is related to the fractions of 3+ and 4+ ions.

Other arguments for the research on TGZ compounds stem from the demonstrated catalytic influences on redox reactions of both several compounds with the pyrochlore structure as well as several Tb containing oxides[10-12]. For certain compounds with the pyrochlore structure it was recently found that an increase in degree of ordering leads to an increased activity towards CO-oxidation[10]. Literature data indicate that several Tb-oxide compounds have highest (catalytic) activity among the other rare earth oxide compounds in CO and NO oxidation[11]. They are also suitable electrode materials for high temperature oxygen sensors[12]. These catalytic effects may be especially advantageous in the case where the materials are applied as surface layers on solid electrolytes in electrocatalytic devices and

sensors.

In summary, this paper deals with the parameters describing mixed conductivity in the system $(Tb_xGd_{1-x})_2Zr_2O_{7+y}$. These are useful data in understanding the behaviour of mixed conducting materials when used as thin electrode layers.

2. DEFECT CHEMISTRY AND CONDUCTIVITY

Compounds containing terbium ions exhibit a variable stoichiometry, caused by the presence of terbium in either 3+ or 4+ valence states. As both ionic and electronic conductivity are dependent on defect concentrations, it is necessary to study the defect chemistry for the TGZ-materials into some detail. The defect structure may be described either in relation to the basic fluorite lattice or, equivalently, to the stoichiometric pyrochlore $A_2B_2O_7$. Using the pyrochlore description the empty oxygen sites have to be considered as part of the regular lattice and can no longer be considered as oxygen vacancies as is the case of the defect fluorite structure. In the pyrochlore description Tb^{4+} ions appear as singly positively charged defects on the rare earth cation sublattice and the corresponding excess oxygen ions are interstitial ions. The number of oxygen interstitials is related to the number of Tb^{4+} cations through:

$$[O_i''] = \frac{1}{2}[Tb^{\cdot}] \qquad (2a)$$

In terms of the parameters used in the composition formula we can write:

$$y = c.x \qquad (2b)$$

where y is the deviation from pyrochlore stoichiometry, x the ratio of Tb ions to the total amount of rare earth ions and c the fraction of Tb in the 4+ valence state. This description, starting from the pyrochlore stoichiometry, is very useful in discussing the electronic conductivity parameters, as it will become clear that Tb^{4+} ions correspond with the charge carriers. If the stoichiometry is expressed relative to the fluorite structure, substitution of Gd^{3+} and Tb^{3+} ions on the cation sites in ZrO_2 now creates singly negatively charged defects, together with oxygen vacancies on the anion sublattice. Tb^{4+} substitutions remain uncharged. The number of oxygen vacancies can be related to the number of 3+ valent cations:

$$[V_O^{\cdot\cdot}] = \frac{1}{2}\left\{[Gd'] + [Tb']\right\} \qquad (3)$$

This description will be used in the defect equilibria to be proposed, because the formulae remain more simple.

The ratio c becomes fixed by the defect equilibrium, that controls the stoichiometry. This equilibrium can be written as:

$$2\,Tb^{x} + O^{x} \rightleftharpoons 2\,Tb' + V_O^{\cdot\cdot} + \frac{1}{2}\,O_{2,g} \qquad (4)$$

from which it follows that:

$$\left(\frac{1-c}{c}\right)^2 . \frac{[V_O^{\cdot\cdot}]}{[O^x]} . pO_2^{1/2} = \text{constant} \qquad (5)$$

So c will be both temperature and pO_2 dependent. Consequently this influences the electronic conductivity to a large extent. Thermogravimetric measurements were carried out to obtain values of c from the weight change of the samples using eq.(2b).

The electronic conductivity in these terbium compounds is supposed to arise from hopping of localized charges and can be described by the (small) polaron model[13-15]. Most studies of this model cited in the literature are related to transition metal oxides. Tuller and Nowick, however, have applied the model to reduced CeO_{2-x} specimen[16]. Criteria mentioned for the

applicability of the small polaron model are a low, thermally activated, mobility (μ) for the electronic charge carriers, a temperature independent Seebeck-coefficient and the possibility of a n ↔ p transition at a given stoichiometry.

In principle both electron and hole conduction can be expected depending on the value of c. Our experiments show that for the TGZ compounds we are dealing with hole conduction. The electronic conductivity (σ_e) can be written as:

$$\sigma_e = c\ N\ z\ e\ \mu \qquad (6)$$

in which z e is the polaron charge. Following the paper by Tuller and Nowick, the mobility has the form:

$$\mu = (1-c)\ \frac{ea^2}{KT}\ \Gamma \qquad (7)$$

The factor Γ describes the jump rate of the hopping process and is different for the cases of adiabatic or non-adiabatic behaviour. In the adiabatic case the electron can tunnel several times between the two sites during an excited state of the phonon system and Γ is given by:

$$\Gamma = \nu_o \exp\left(\frac{-\Delta H_\mu}{RT}\right) \qquad (8)$$

where ν_o should correspond to the frequencies of the phonons involved. On the contrary, in the non-adiabatic case, the chance of tunnelling during the excited state is small and Γ reads:

$$\Gamma = \frac{J^2}{\hbar}\ \frac{1}{(\Delta H_\mu kT)^{1/2}}\ \exp(-\Delta H_\mu / kT) \qquad (9)$$

So a $T^{-3/2}$ dependence is found for the pre-exponential factor of the mobility instead of a T^{-1} dependence in the adiabatic case. It is, however, difficult to discriminate between these two temperature dependences on the basis of experimental data. Therefore, rather the frequency of the hopping proces (ν_o) will be calculated using the adiabatic formula (8) for our data and this will be compared with results of infrared spectral studies[17].

3. EXPERIMENTAL METHODS

3.1. Methods.

All materials were prepared by means of a wet chemical synthesis in order to obtain fine grained and homogeneous powders. A viscous solution of citrate complexes of the constituent metalions was thermolysed and the product was calcined[18]. The calcination was performed at 800°C for 6 hours. Then the powders were pressed isostatically at 400 MPa and sintered into dense ceramics at 1550°C during 40 hours. Specimen with x ranging from 0.0 to 1.0 and relative densities of 93% or more were obtained. Specimen with a high Tb concentration ($x \geq 0.3$) appeared to be rather brittle, showing subtle cracks, probably caused by changes in stoichiometry during heating and cooling in the furnace.

Compounds with $x \leq 0.2$ were either quenched from temperatures above the order-disorder temperature (1550°C for $Gd_2Zr_2O_7$) or annealed below that temperature to obtain specimen with different degree of order.

For X-ray diffraction (XRD), X-ray fluorescence (XRF) and thermogravimetric analysis (TGA) experiments, part of the ceramic material was crushed and milled. The micro-structure of polished and thermally etched samples was examined using scanning electron microscopy (Jeol JSM 35 CF). The average grain size of the specimen was determined with the line intercept method using corrections according to the method of Mendelsohn[19].

Electrical measurements were carried out on

disc-shaped samples with thicknesses of 0.6 to 1.5 mm and diameters of 6 to 10 mm. The samples were polished with 1 μm Al_2O_3 and cleaned in ethanol. Platinum electrodes were sputtered on both sides of the discs. An average thickness of 0.2 μm appeared to give porous but continuous electrodes after sintering at 950°C for 2-3 hours. These electrodes were stabilised before use by a heat treatment at 750°C for two days, followed by an electrical treatment at 1V and at 1 kHz for 5 minutes.

XRD experiments were carried out using a Philips powder diffractometer PW 1330 and Cu-Kα radiation.

The composition of the compounds was checked by XRF analysis and was found to deviate less than 1% from the desired composition.

TGA was carried out on a Cahn RG balance. Runs from 350-1000°C were performed in steps, allowing the sample to fully equilibrate with its ambient atmosphere and temperature. Oxygen partial pressures between 10^{-5} and 1.0. atm were applied, using mixtures of $N_2$and O_2. The exact oxygen partial pressure was monitored using a stabilized zirconia oxygen sensor and a reference gas.

The ionic transport number (t_i) was determined with the e.m.f. method in a concentration cell. Air and pure oxygen were used as the reference gases[27].

The conductivity experiments were carried out using frequency dispersion analysis (1 mHz-1 MHz) with a Solartron 1174 FRA, coupled to a personal computer (HP85). Measurements were carried out between 250 and 750°C with oxygen partial pressures between 10^{-5} and 1.0 atm. A constant linear gas flow of about 20 mm/min was applied close to the sample. The sample was spring-loaded between platinum foils in the sample holder. The gases used were either taken from bottles with standard gases or mixed, using Inacom mass flow meters. The oxygen partial pressure was registered using a stabilized zirconia oxygen sensor.

3.2. Experiments under reducing atmosphere.

For the interpretation of the electronic conductivity according to eq. 6, it is necessary to have information of the charge carrier concentration. In principle Seebeck-coefficient determinations might be useful, but in case of mixed conducting materials, the experimental results are always composed of both an electronic and ionic part[20]. Therefore we have used another, independent, way to determine the concentration of Tb^{4+} ions.

It was found that under strongly reducing conditions all Tb^{4+}-ions could be converted to Tb^{3+} ions, which results in the stoichiometric compounds $A_2B_2O_7(y=0)$. Upon reoxidation the weight change of the sample can be related to the value of y and consequently the number of charge carriers can be calculated from eq. 3b for each experimental condition.

Confirmation of this state of reduction to stoichiometric pyrochlore was obtained by: i) a colour change of the TGZ sample from brown to white, comparable with the colour of pure $Gd_2Zr_2O_7$; ii) a constant weight of the sample between 450 and 950°C; iii) the fact that a single TGA run[21] up to 1300°C asymptotically approached a stoichiometry corresponding with the one we found under reducing conditions between 450 and 950°C; iv) the fact that impedance plots of A.C. conductivity measurements on the samples under the same conditions, were similar to plots obtained for $Gd_2Zr_2O_7$. Hence it can be concluded that the electronic conductivity has vanished under these strongly reducing conditions.

The reducing atmosphere was established with a gas mixture of 1% CO and 99% CO_2. According to the equilibrium reaction between these gases, oxygen partial pressures in the range 10^{-14} -10^{-20} atm are obtained in the temperature interval between 650 and 950°C[22]. Specimen for TGA and conductivity measurements were

reduced in this atmosphere above 650°C. For measurements below 650°C the gas mixture was first brought in equilibrium at high temperature before being applied to the furnace containing the specimen. Even if deviations from equilibrium should occur, it was ascertained that a sufficiently low pO_2 was reached to obtain the desired degree of reduction of the sample.

4. RESULTS

4.1. XRD and microstructure.

For TGZ compositions with $x \geq 0.2$ and for compositions with $x \leq 0.2$ quenched from above the order-disorder transition temperature, the fluorite structure was found. $Gd_2Zr_2O_7$, annealed at temperatures between 1200 and 1500°C, clearly shows the superstructure diffraction peaks belonging to the pyrochlore structure. For TGZ10 faint superstructure diffraction peaks are present, indicative of partial ordering. The order-disorder transition was extensively studied for these compounds, using electron diffraction and imaging techniques in the electron microscope. Results of this study will be published elsewhere[7].

In Fig.1 the lattice parameter for the fluorite structure is presented. In case of materials with pyrochlore ordering, the value of the fluorite subcell is taken for comparison. It can be seen that the value of the lattice parameter decreases continuously going from TGZ0 to TGZ100. This is in accordance with the smaller size of the Tb^{3+} ion compared to Gd^{3+}. Another influence on the value of the lattice parameter might come from the presence of Tb^{4+} with even smaller ionic radius and the additional amount of oxygen ions which are necessarily incorpo rated. This does not play a role, however, because it was found that the lattice parameters of both a reduced sample (c and y both 0) and a sample equilibrated in air

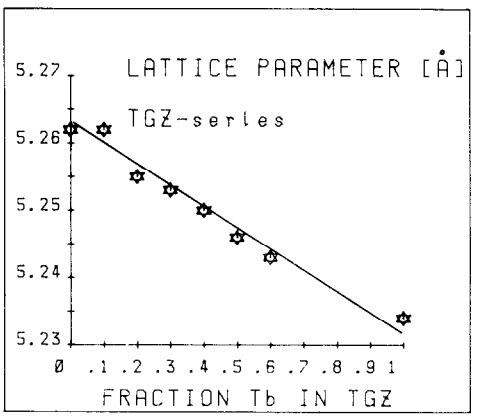

Fig.1. Lattice parameter of the fluorite structure for the compositions TGZ.

at 600°C (c=0.14, y=0.056, see section 4.2) were equal within measurement error. Obviously, these effects seem to compensate each other. Hence it was concluded that the variations of the lattice parameter with x are mainly caused by the difference in ionic radii for Gd^{3+} and Tb^{3+}.

Average grain sizes for specimen sintered at 1550°C for 24-40 hours were in the range 2-4 μm. The specimen of TGZ0, quenched from 1700°C, had grain sizes of about 12 μm and a single specimen of TGZ40, annealed at 1700°C for 60 hours had an average grain size of 20 μm. This latter specimen was prepared to check whether the electronic conductivity is dependent on the grain size. Residual porosity in all cases was found to be mainly present at the grain boundaries.

4.2. Thermogravimetric analysis.

TGA measurements were carried out for the compounds with x=0, x=0.40 and x=1.00. For TGZ0 no weight changes were detected, neither when the temperature was varied, nor when varying pO_2 conditions were applied. Consequently, this compound is in its electrolytic domain under all experimental conditions.

For TGZ40 and TGZ100 a continuous decrease in weight with increasing temperature was

found. Below 350°C specimen could not be equilibrated in reasonable times. Tb^{4+} fractions (c) could be calculated and results for measurements in air between 350 and 950°C are presented in Fig.2. The absolute values for c were derived from the weight changes with respect to the reducing conditions, as was described in section 3.2.

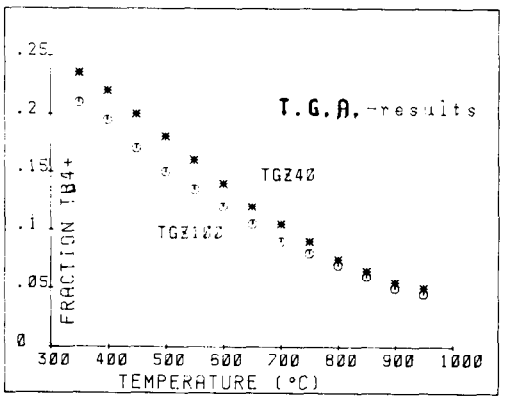

Fig.2. Tb^{4+} fraction versus temperature determined from t.g.a. results in air, for TGZ40 and TGZ100.

TGA measurements in the pO_2 range 10^{-5}-1.0 atm showed that the Tb^{4+} fraction decreased with decreasing pO_2, but the measurements were not sensitive enough to provide reliable information on the validity of the proposed defect equilibrium (4) and the equilibrium constant (5).

It can be seen from Fig.2 that the Tb^{4+} fraction never exceeds the value of 0.25 in the temperature interval 350-950°C up to pO_2=1.0 atm. So the electronic conductivity will be p-type for all experimental conditions. Differences between the curves for TGZ40 and TGZ100 are not quite significant and hence an important conclusion is that the Tb^{4+} fraction is almost independent of the total fraction of Tb in the compound. The equilibrium constant seems to be determined predominantly by the structure and temperature, and not by the composition.

4.3. Transport number determinations.

Concentration cell determinations of the ionic transport number ($t_i = E_{measured}/E_{Nernst}$) were carried out for all TGZ compositions as a function of temperature. A few of these curves are presented in Fig.3. For TGZ0 and TGZ10 no deviation from fully ionic conductivity could be detected within the measurement error of about 0.05 in t_i. For the compositions with $x \geq 0.2$ a gradual decrease is observed on increasing Tb concentration.

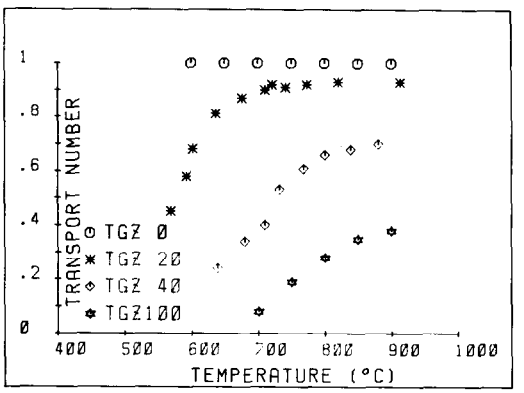

Fig.3. Transportnumber (t_i) versus temperature for compositions TGZ.

The decrease of t_i with decreasing temperature may be related to the observed increase in the number of charge carriers for electronic conductivity (Tb^{4+}) with decreasing temperature, but can also be the result of differences in activation enthalpies for the ionic and electronic conductivities.

Curves of t_i versus temperature for $x \geq 0.2$ show a pronounced bend at a given temperature, below which no reliable values of t_i can be obtained. This behaviour is probably a consequence of the combined transport of both oxygen and electrons through the material, followed by electrode polarization at the mixed conductor-gas interface[3,23]. In order to obtain separated values of ionic and electronic conductivity below the temperature of the bend, another

independent method was applied, which will be discussed in section 4.5.

No differences were observed between the concentration cell potentials of a standard specimen TGZ40 and of the sample annealed at 1700°C for 60 hours, in which the grains were about 6 times larger. Therefore, there are no grain boundary effects that play a significant role in the conductivity mechanism.

4.4. Conductivity measurements.

Impedance plots were obtained for all compositions between 250 and 750°C in air. For TGZ40 and TGZ100 the oxygen partial pressure was varied between 10^{-5} and 1.0 atm and supplementary measurements were carried out under reducing conditions, as was explained in section 3.2. A varying degree of dispersion was obtained as a function of x, temperature and pO_2.

The interpretation of the impedance plots was based on the assumptions that the ionic and electronic conductivities can be represented by parallel branches in the equivalent circuit and that the ionic resistivity contains a bulk, grain boundary and interfacial part, R_b, R_{gb} and R_{el} respectively. The exact form of the interfacial ionic impedance is not discussed here, but we will assume that a pure resistance value will be found at relatively low frequencies. This results in the electrical equivalent circuit given in Fig.4, which is comparable with the circuit used by Gogé et al. for the interpretation of conductivity measurements on Sm and Yb stabilized zirconia[24]. The impedance plots from which we derived the circuit have generally the form given in Fig.5. Table I records the intercept values R_1, R_2 and R_{DC} of these plots in terms of the separated ionic and electronic resistances.

For $t_i=1$ ($R_e=\infty$) the circuit reduces to the one characteristic for pure oxygen ion conductors, while for $t_i \to 0$ the resulting resistances approach the value of Re. A decrease of t_i becomes first manifest in the value of R_{DC} and on further decrease of t_i in the values of R_2 and R_1. The once observable semicircles for grain boundary and electrode polarization accordingly vanish. An example of an impedance plot for TGZ40 is given in Fig.6. The depression of the semicircle does not follow from the

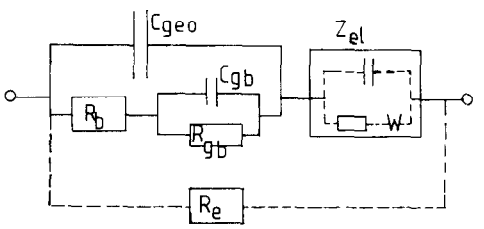

Fig.4. Equivalent circuit for mixed conductivity in the compositions TGZ: C_{geo}= geometric capacitance, R_b= ionic resistance, R_{gb}= grain boundary ionic resistance, C_{gb}= grain boundary capacitance, Z_{el}= electrode impedance, R_e= electronic resistance.

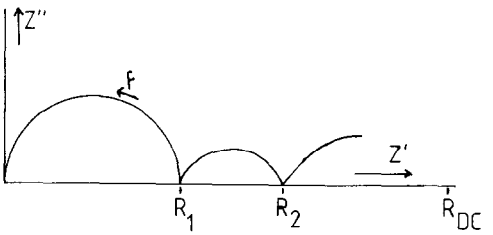

Fig.5. General impedance plot for the equivalent circuit given in fig.4.

Table I. Interpretation of the intercept values of the impedance plots in accordance with the equivalent circuit of Fig.4.

	R_1	R_2	R_{DC}
$t_i=1$	R_b	R_b+R_{gb}	$R_b+R_{gb}+R_{el}$
$t_i<1$	$(\frac{1}{R_b}+\frac{1}{R_e})^{-1}$	$(\frac{1}{R_b+R_{gb}}+\frac{1}{R_e})^{-1}$	$(\frac{1}{R_b+R_{gb}+R_{el}}+\frac{1}{R_e})^{-1}$
$t_i<<1$	R_e	R_e	R_e

equivalent circuit, but results from a spread in relaxation times, probably connected with stoichiometry variations of the sample under A.C conditions.

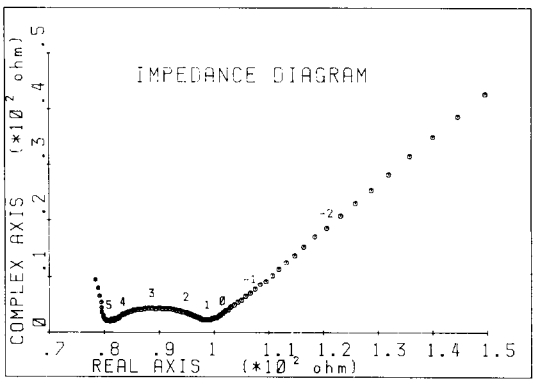

Fig.6. Experimental impedance plot for TGZ40 at 700°C in air.

Using the equivalent circuit of Fig.4, R_2 may be interpreted as the total bulk resistance of the sample and σ_2 will denote the total bulk conductivity. For a number of compounds Arrhenius diagrams for σ_2 at pO_2=0.21 atm are plotted in Fig.7. Generally no straight lines are observed, indicating that at least two conductivity processes play a role and/or that the stoichiometry varies within the temperature interval. For $x \geq 0.4$ the conductivity increases significantly, especially at the lower temperatures. This is accompanied with a gradual decrease in activation enthalpy and is a result of the predominant electronic character of the conductivity at larger x. A more detailed interpretation of the conductivity behaviour will be given after the separation of σ_2 in its electronic and ionic contributions.

Straight lines in Arrhenius diagrams are obtained for TGZ40 and TGZ100 for measurements under reducing conditions (c and y both 0). This holds both for the bulk and the grain boundary conductivity. In Table II values for

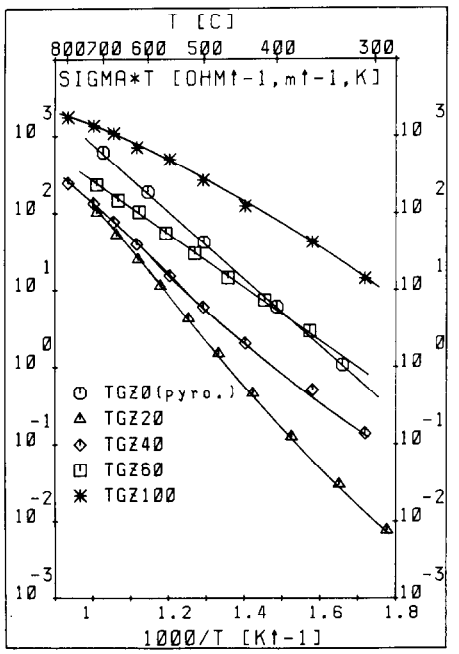

Fig.7. Arrhenius diagrams for conductivities of samples TGZ measured in air.

the activation enthalpy ΔH and pre-exponential factor σ_o are listed together with corresponding values for TGZ0 and TGZ10, determined from measurements in air. The latter two compounds were found to be fully ionic conductors at all pO_2. The conductivity parameters of TGZ40 and TGZ100 under reducing conditions are quite comparable with the ones for the fluorite type TGZ0 and TGZ10, indicating that we are dealing with purely ionic conduction.

5. DISCUSSION

5.1. Separation in ionic and electronic contributions.

In general the electronic and ionic contributions to the total conductivity can be obtained separately, using the transport num-

Table II. Values of ΔH and σ_o for ionic conductivity a) determined in air; b) determined at $pO_2 = 10^{-15}$-10^{-20} atm. The relative error in ΔH-values is about 3-5%.

compound	bulk		grainboundary	
	ΔH[kJ/mol]	$\sigma_o[\Omega^{-1}m^{-1}K]$	ΔH[kJ/mol]	$\sigma_o[\Omega^{-1}m^{-1}K]$
TGZ0 - pyrochlore[a]	84	2.0×10^7	140	2×10^9
fluorite[a]	112	1.0×10^8	*)-	-
TGZ10- pyrochlore[a]	104	3.5×10^7	124	8×10^8
fluorite[a]	115	2.3×10^8	135	5×10^9
TGZ40 [b]	121	2.6×10^8	136	5×10^9
TGZ100[b]	126	3.1×10^8	135	5×10^9

*) For TGZ0 in the fluorite phase no separate grainboundary contribution in the impedance plots was observed, due to the large grain size, as a result from the temperature treatment at 1700°C

bers measured in concentration cell experiments. Although these t_i values are average values for an oxygen partial pressure range between, in our case 0.21 atm and 1.0 atm, the obtained values are used as a good approximation for conductivity ratio's measured at fixed pO_2. Reliable t_i-values were only obtained in a limited temperature range as was explained in section 4.4. In this temperature range the ionic and electronic conductivities were calculated from R_2 values in the impedance plots, using:

$$t_i = \frac{\sigma_i}{\sigma_i+\sigma_e} = \frac{R_2}{R_b+R_{gb}} = 1 - \frac{R_2}{R_e} \qquad (11)$$

For temperatures lower than the bends in the t_i diagrams of Fig.3 we used the following different procedure. It is assumed that the ionic conductivity for the mixed conducting materials is in first approximation independent of the oxygen partial pressure. Then the ionic and electronic contributions can be obtained separately at all pO_2 by subtracting the ionic conductivity, determined under reducing conditions (when the electronic conductivity has vanished) from the total conductivity (σ_2). The validity of this procedure is discussed below. Equation (2) shows that the oxygen vacancy concentration follows from $[Gd^{3+}]$ and $[Tb^{3+}]$. Relative changes in $[V_O^{\cdot\cdot}]$ are for all x much smaller than changes in the electronic charge carrier concentration $[Tb^{4+}]$, because the Tb^{4+} fraction is always small (<0.25). So relative changes in the electronic conductivity are dominant over changes in the ionic conductivity, due to stoichiometry variations (y). Secondly (applying the relations given in Table I) the same values for R_e have been obtained by subtracting values of ionic bulk resistance from R_1 and ionic bulk and grain boundary resistances from R_2 (provided R_1 and R_2 are well separated). Finally, both methods, used to determine t_i, show to overlap in the region where the concentration cell measurements give reliable results. This is illustrated in fig.8, where ionic transport numbers, determined from both methods, are given for TGZ40. It can be seen that the concentration cell method gives too low values when $t_i \leq 0.5$.

5.2. Electronic conductivity and mobility.

From the results of the ionic transport numbers, it is concluded that the onset of electronic conductivity as a function of composition (x) for the TGZ materials is somewhere between x=0.10 and x=0.20. When we consider the cations of the fluorite lattice, this implies that the onset of electronic conductivity turns up for a fractional occupation of the cation

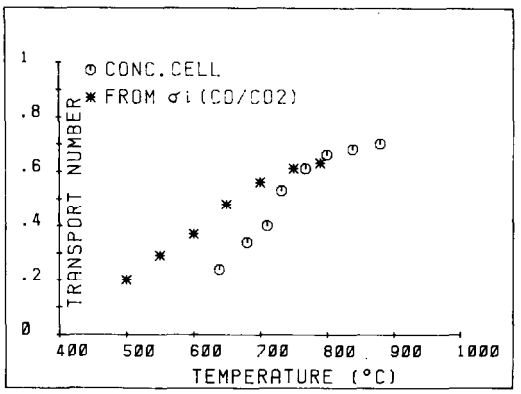

Fig.8. Comparison of ionic transport numbers for TGZ40 obtained from concentration cell measurements and from measured ionic conductivities under reducing conditions.

lattice by Tb between 0.05 and 0.10. Suppose the conduction mechanism is based on the presence of chains consisting of nearest neighbour Tb ions, then percolation theory predicts a value of 0.195 for the critical percolation probability[25]. This value is clearly larger than we found. No different result is obtained, if we consider the ordered pyrochlore structure, since is was pointed out by Scher and Zallen[26] that the critical probability density, which must be the same for the fluorite and pyrochlore structure, is independent of the lattice structure. The disagreement between experiment and theory may imply that either grain boundary segregation and conductivity occurs or that the conduction pathway involves also electron jumps other than between Tb nearest neighbour ions.

Transport number measurements on samples with different grain sizes showed that grain boundaries do not play a significant role. Arguments for the existence of different types of jumps, stem from the variation of the activation enthalpy, as will be demonstrated below.

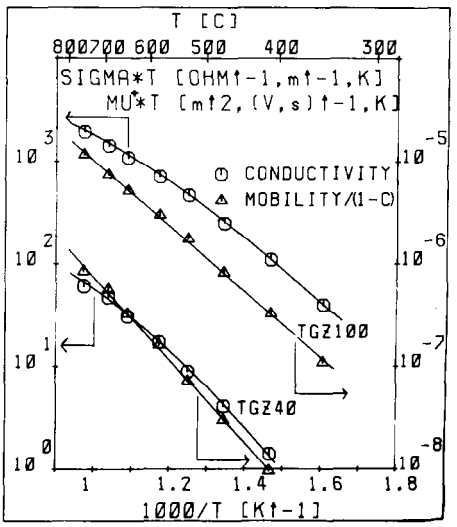

Fig.9. Electronic conductivity (σ_e) and stoichiometry independent mobility $\mu^+=\mu/(1-c)$ for TGZ40 and TGZ100 in Arrhenius diagrams.

Fig.9 shows both the electronic conductivity σ_e, and the stoichiometry independent mobility, $\mu/(1-c)$, in an Arrhenius diagram for TGZ40 and TGZ100. Due to stoichiometry variations in the temperature interval of the conductivity measurements the curves of σ_e versus 1/T appear to be concave towards the origin. Values $\mu/(1-c)$, which do not contain these stoichiometry effects, give reasonable straight lines, indicating that the mobility is indeed thermally activated and has values well below the upper-limit of 10^{-5} m^2/Vs for small polaron behaviour. Therefore it seems reasonable to apply this model to the electronic conductivity in the TGZ materials. In Fig.10 the activation enthalpies for the mobility are plotted versus the quantity $N^{-1/3}$, where N is the concentration of Tb sites. Since $N^{-1/3}$ represents the average distance between Tb sites, it can be concluded that the activation enthalpy increases linearly on in creasing average dis-

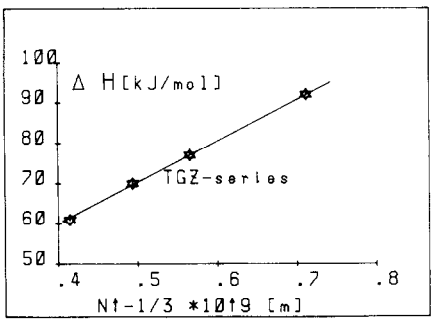

Fig.10. Activation enthalpies for the stoichiometry independent mobilities versus the average distance between Tb sites.

tance. Considering nearest neighbour jumps only, a constant activation enthalpy would be expected, once the concentration of Tb ions has exceeded the percolation treshold, because the nearest neighbour distance in the infinite percolation cluster is determined only by the lattice parameter. Hence, this is an indication that the conduction mechanism is not only based on electron hopping between Tb nearest neighbour sites, but on hopping between Tb sites with larger mutual distance too. Each kind of jump is described by its own activation enthalpy, that increases for larger mutual distances. Obviously, this results in a decrease in activation enthalpy for increasing Tb-concentration.

For TGZ100 we can assume that predominantly nearest neighbour Tb ions are involved in the conduction process. Using this nearest neighbour intersite distance (1/2 $\sqrt{2}$ * 5.25 Å) the polaron frequency ν_o can be calculated from eq.7 and eq.8. The resulting value of about 10^{13} Hz is in accordance with the experimental infrared absorption spectra[17], that show highest absorption between 250 and 500 cm^{-1}. Tuller and Nowick found a similar value in the case of CeO_{2-x}[16], which indicates that the adiabatic small polaron model is plausible.

5.3. pO_2 dependence for σ_e.

Using the relationships between the oxygen partial pressure and c (eq.5) and between the electronic conductivity and c (eq.6) a relation can be found for the variation of the electronic conductivity with the variation in pO_2 in the case of TGZ100

$$\frac{\partial \log \sigma_e}{\partial \log pO_2} = \frac{1-2c}{4+2c} \qquad (12)$$

This relation shows that there is no linear relationship between log σ_e and log pO_2, but that the slope depends on c and ultimately for c→0 reaches the value 0.25 ($\sigma_e \propto pO_2^{1/4}$). For smaller values of x approximately the same relation (12) holds.

A plot of log σ_e versus log pO_2 at 700°C is given for TGZ40 in Fig.11. Average values of the slope of log σ_e versus log pO_2 at 700°C within the pO_2 interval $2x10^{-5}$-1.0 atm amount 0.15 (±0.03) and 0.21 (±0.03) for TGZ100 and TGZ40 respectively. For both compositions the parameter c is in the order of 0.10, so a theoretical average slope of 0.19 was expected. This indicates that the proposed defect equilibrium (4) provides a reliable description of the behaviour of the solid solutions.

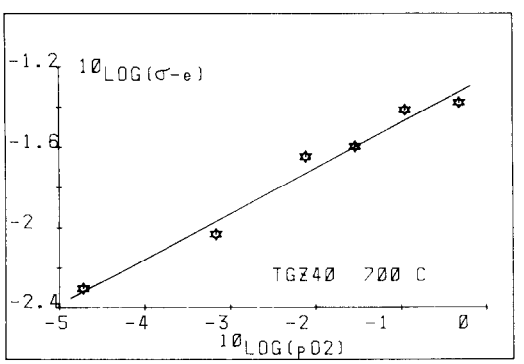

Fig.11. Experimental relation between the electronic conductivity and oxygen partial pressure for TGZ40 at 700°C. The slope of the drawn line is 0.21 ± 0.03.

5.4. Ionic conductivity.

In Fig.12 values of ΔH and σ_o for ionic conductivity are presented for the whole TGZ series. It can be seen that values of ΔH and σ_o for the solid solutions in the fluorite phase form a consistent set. A slight decrease of both ΔH and σ_o going from TGZ100 to TGZ0 can be attributed to an increase in the degree of ordering, which was also seen in the electron diffraction patterns[7]. For TGZ0 and TGZ10 much lower values of ΔH and σ_o are found when the compounds have been annealed below the order-disorder temperature and which results in formation of the pyrochlore structure. This supports our previously developed model which explains the decrease in ΔH and σ_o for the transition from the fluorite to the pyrochlore structure[5-8]. This model is based on the existence of preferential diffusion pathways with a low barrier energy in the pyrochlore structure. Moreover, it was suggested that antiphase boundaries in the domain-like structure possibly contribute to the conductivity mechanism, as ionic arrangements at these boundaries provide continuous pathways with anticipated low barrier energy[8].

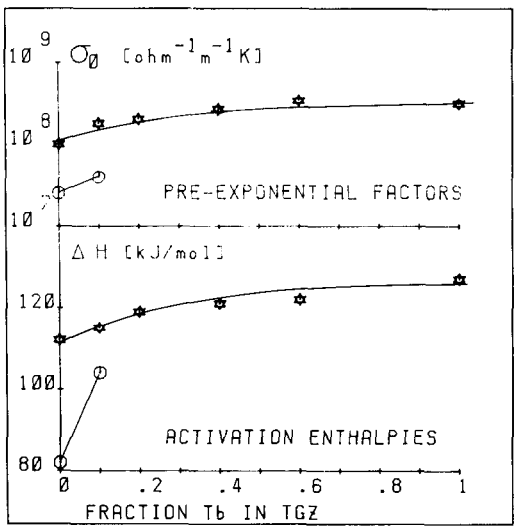

Fig.12. Activation enthalpies and pre-exponential factors for ionic conductivity are given for the TGZ series. The values result from conductivity measurements i) in air for the purely ionic conductors TGZ0 and TGZ10 ii) under reducing conditions for TGZ40 and TGZ100 iii) in air, combined with ionic transport numbers, for TGZ20 and TGZ60.
○ pyrochlore, ● fluorite structure.

6. CONCLUSIONS

1. Compositions $(Tb_xGd_{1-x})_2Zr_2O_{7+y}$ form a solid solution series with linear decreasing fluorite lattice parameter on increasing x. For $x \leq 0.20$ indications of pyrochlore order are found, depending on the heat treatment applied.
2. The ionic conductivity of all compositions with the fluorite structure is about $10^{-1}\Omega^{-1}m^{-1}$ at 700°C and is 7 times smaller than for well ordered $Gd_2Zr_2O_7$ (pyrochlore). Our conductivity model based on the influence of ordering can account for the differences in ΔH and σ_o found for the fluorite and pyrochlore structure.
3. The p-type electronic conductivity increases with the amount of Tb ions. It can be described by a small polaron hopping mechanism. The results suggest that jumps between nearest neighbours Tb ions in the lattice as well as between Tb ions at larger mutual distances are involved in the conduction mechanism. Mobilities are thermally activated and are in the order 10^{-10}-10^{-8} m^2/Vs at 700°C. The charge carrier concentration (Tb^{4+}) is temperature and oxygen partial pressure dependent. The maximum obtainable Tb^{4+} fraction is 0.25 and is almost composition independent.

REFERENCES

1. E.J.L. Schouler, Solid State Ionics 9/10 (1983) 945.
2. S.P.S. Badwal, J.Electroanal.Chem. 46 (1983) 425.
3. M.P. van Dijk, J.H.H. ter Maat, G. Roelofs, H. Bosch, G.M.H. van de Velde, P.J. Gellings and A.J. Burggraaf, Mat.Res.Bull. 19 (1984) 1149.
4. Y. Takasu, T. Sugino, Y. Matsuda, J.Appl.Electrochem.14 (1984) 79.
5. T. van Dijk, K.J. de Vries and A.J. Burggraaf, Phys.Stat.Sol. (a) 58 (1980) 115
6. M.P. van Dijk, K.J. de Vries and A.J. Burggraaf, Solid State Ionics 9/10 (1983) 913.
7. M.P. van Dijk, F.C. Mylhof and A.J. Burggraaf, to be published.
8. M.P. van Dijk, A.N. Cormack, A.J. Burggraaf and C.R.A. Catlow, to be published.
9. D. Michel, M. Perez Y Yorba and R. Collongues, Mat.Res.Bull. 9 (1974) 1457.
10. J.H.H. ter Maat, M.P. van Dijk, G. Roelofs, H. Bosch, G.M.H. van de Velde, P.J. Gellings and A.J. Burggraaf, Mat.Res.Bull. 19 (1984) 1271.
11. Y. Takasu, S. Nishibe and Y. Matsuda, J.Cat. 49 (1977) 236.
12. C.M. Mari and G. Terzaghi in: Proceedings of the International Meeting on Chemical Sensors, Fukuoka (Jpn), eds. T. Seijama et al. (Kodanska, Elsevier, 1983) pp. 273-278.
13. I.G. Austin and N.F. Mott, Advances in Physics 18 (1969) 41.
14. A.J. Bosman and H.J. van Daal, Advances in Physics 19 (1970) 1.
15. G. Oversluyzen, Ph.D.Thesis, Eindhoven, University of Technology, The Netherlands (1983) p.11.
16. H.L. Tuller and A.S. Nowick, J.Phys.Chem. Solids 38 (1977) 859.
17. W.E. Klee and G. Weitz, J.Inorg.Nucl.Chem. 31 (1969) 2367.
18. M.A.C.G. van de Graaf, T. van Dijk, M.A. de Jongh and A.J. Burggraaf, Science of Ceramics, Vol.9, ed. K.J. de Vries (De Nederlandse Keramische Vereniging, Enschede, 1977) pp. 75-84.
19. M.I. Mendelsohn, J.Amer.Ceram.Soc. 52 (1969) 443.
20. H. Holtan, P. Mazur and S.R. de Groot, Physica 19 (1953) 1109.
21. Thanks are due to Mr. L. Boon of Eindhoven University of Technology, who carried out this t.g.a. run for us.
22. Handbook of Chemistry and Physics.(CRC Press, Inc., Cleveland, Ohio)
23. J. Fouletier, E. Mantel and M. Kleitz, Solid State Ionics 6 (1982) 1.
24. M. Gogé, G. Létisse and M. Gouet, Solid State Ionics 9/10 (1983) 937.
25. V.K.S. Shante and S. Kirkpatrick, Adv. Advances in Physics 9/20 (1971) 325.
26. H. Scher and R. Zallen, J.Chem.Phys. 53 (1970) 3757.
27. K.J. de Vries, T. van Dijk and A.J. Burggraaf, in: Proceedings of the International Conference on Fast Ion Transport in Solids, Electrodes and Electrolytes, Lake Geneva (U.S.A.), eds. P. Vashishta, J.N. Mundy and G.K. Shenoy (North-Holland, Amsterdam,1979) pp. 679-682.